3828 *Macromolecules* **2010**, *43*, 3828–3836
DOI: 10.1021/ma100027b

Macromolecules
ARTICLE

Interfacial Segregation in Polymer/Fullerene Blend Films for Photovoltaic Devices

David S. Germack,[†] Calvin K. Chan,[†] R. Joseph Kline,[†] Daniel A. Fischer,[†] David J. Gundlach,[†] Michael F. Toney,[‡] Lee J. Richter,*[,†] and Dean M. DeLongchamp*[,†]

[†]*National Institute of Standards and Technology, Gaithersburg, Maryland 20899, and* [‡]*Stanford Synchrotron Radiation Lightsource, Menlo Park, California 94025*

Received January 5, 2010; Revised Manuscript Received March 3, 2010

ABSTRACT: It has recently been shown that surface energy effects can cause selective segregation at the active layer interfaces of a bulk heterojunction (BHJ) organic photovoltaic device. The active layer interface composition has been suggested to impact device performance. In this study changes in the BHJ vertical composition profile of BHJ active layers cast on two hole transport layers (HTL) with significantly different surface energies (γ) are characterized using spectroscopic ellipsometry and near-edge X-ray absorption fine structure spectroscopy. Changes in the HTL γ are shown to significantly affect the BHJ interfacial segregation at the buried interface near the HTL while the composition near the free surface (air) of the BHJ is unaffected. Despite the significant differences in vertical segregation at the HTL interface, the performances of the resulting organic photovoltaic devices were relatively similar.

Introduction

Organic photovoltaics (OPVs) are a promising class of devices for producing renewable electricity. The thin-film geometry of these devices makes them amenable to inexpensive and high-throughput production methods (printing), and the organic materials employed in their construction impart mechanical robustness.[1] OPV devices can be prepared on a wide range of flexible substrates ranging from thin plastic films[2] to fibers and wires,[3,4] enabling unique form factors for the device architecture.

In a bulk heterojunction (BHJ) type OPV device, the BHJ active layer has many roles. It must absorb light, generate excitons, separate the excitons into charge carriers (holes and electrons), and transport the charge carriers to their respective electrodes.[5] Each of these processes requires specific electronic and structural characteristics that must be optimized. The structure of the BHJ active layer forms dynamically during its solidification from a solution; it depends strongly on processing conditions and materials properties of the components such as their mutual miscibility, surface energies, and crystallinity.[6] The most widely studied OPV BHJ blend consists of a poly(3-hexylthiophene) (P3HT) absorber and 1-(3-methoxycarbonyl)-propyl-1-phenyl-[6,6]C_{61} (PCBM) electron acceptor. This system can yield devices with a power conversion efficiency in excess of 4% under optimized conditions.[7] Initial work on optimizing the P3HT:PCBM system has focused on processing conditions such as the choice of solvent, deposition method, deposition temperature, drying rate, and annealing method, with the goal of forming a bulk morphology of small, highly interpenetrating, continuous domains of the absorber and acceptor phases. One area of optimization that has only recently received attention is the composition and structure of the BHJ external interfaces.

We recently reported the interfacial compositions of P3HT:PCBM blend films cast on model substrates with surface energies (γ) tailored by self-assembled monolayers (SAMs).[8] Using surface sensitive near-edge X-ray absorption fine structure (NEXAFS) spectroscopy with a delamination procedure that exposed buried interfaces, we found that on high γ substrates, such as SiO_2, the buried interface was selectively enriched with the PCBM phase, whereas on low γ substrates the buried interface was enriched with P3HT. The air interface (free surface) of the BHJ blend was always enriched with the P3HT, consistent with air being a low γ surface. These observations were understood in terms of simple interfacial free energy arguments and reports in the existing literature.[9−12] As model surfaces and non functional HTLs were used, the relationship between interfacial segregation and OPV device performance was not quantified.

Yang and co-workers recently reported P3HT:PCBM blend devices with an inverted architecture, where the cathode is at the buried interface and the anode is applied to the air interface (Scheme 1b). These devices achieved an increased power conversion efficiency (η) over a conventional architecture, where the anode is at the buried interface and cathode applied to the air interface (Scheme 1a).[13,14] The enhanced performance of the inverted architecture was attributed to a surface energy-induced segregation of the blend components. X-ray photoelectron spectroscopy (XPS) revealed that the air interface of the blend film was P3HT-rich, whereas the buried interface atop a high γ substrate was PCBM-rich. In the conventional device, such segregation would unfavorably locate the hole transporting phase of the active layer adjacent to the cathode and the electron transporting phase adjacent to the anode. In an inverted device, however, the appropriate phases would contact the appropriate electrodes for charge extraction. Yang and co-workers speculated that PCBM enrichment also occurred at the PEDOT:PSS HTL that is often used in conventional devices. This speculation was based the moderately high γ of the PEDOT:PSS HTL, but conclusive XPS measurements on the buried interface were not possible due to cohesive failure of the PEDOT:PSS layer during delamination which resulted in PEDOT:PSS residue that could not be removed. Even though a direct correlation to performance could not be shown, this work suggests that interface

*Corresponding authors. E-mail: deand@nist.gov (D.M.D.); lee.richter@nist.gov (L.J.R.).

 Published on Web 03/25/2010

Scheme 1. Illustration of the Conventional Device Architecture (a), Inverted Device Architecture (b), and the Structures of P3HT and PCBM

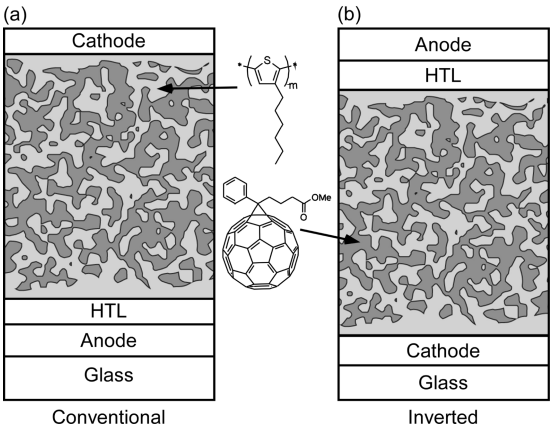

composition control presents an opportunity for improving OPV device performance.

An alternative to inverting the device stack is to lower the surface energy of the HTL, causing the buried interface to become enriched with P3HT and optimizing the anode−BHJ interface in a conventional device architecture. In this report, we evaluate this strategy with detailed structure characterization methods and electrical performance measurements. The lower γ surface is provided by a novel, poly(thienothiophene):Nafion (PTT:Nafion)-based HTL (see Scheme 2) with a static water contact angle of ≈104°. The PTT:Nafion work function of 5.4 ± 0.1 eV is similar to the 5.0 ± 0.2 eV work function of PEDOT:PSS so that any differences in device performance between OPV devices prepared on the two HTLs due to the work function matching with the BHJ layer are minimized. We compare the structure of P3HT:PCBM films cast atop PTT:Nafion to films cast atop PEDOT:PSS using spectroscopic ellipsometry (SE) which permits a nondestructive evaluation of the vertical composition profile that does not rely on delamination. Because SE interpretation is model dependent, we validated the interface composition results from SE with NEXAFS spectroscopy and the P3HT anisotropy with grazing incidence X-ray diffraction (GIXD). We find that the buried interface composition changes dramatically with HTL surface energy. This change, however, did not have a significant effect on OPV power conversion efficiency in our devices. These results have important implications for the design of OPV devices (inverted vs normal) and for the design of HTLs for improved performance.

Results and Discussion

Spectroscopic Ellipsometry. In this article, variable angle SE is used as the primary tool to quantify the vertical compositional profile of the BHJ active layer. In a standard SE measurement the complex ratio of the reflection amplitudes of polarized light with the electric field in the plane of incidence (r_p) and perpendicular to the plane of incidence (r_s) is measured in terms of the ellipsometric parameters Ψ and Δ as described in eq 1.

$$\frac{r_p}{r_s} \equiv \tan(\Psi)e^{i\Delta} \quad (1)$$

This ratio can be measured extremely accurately. With the use of appropriate physical models, the SE data can be used to determine the vertical compositional profile of complex multilayer systems. The dielectric functions of P3HT and PCBM are distinct and should permit robust assignment of a composition profile. However, the dielectric function can

Scheme 2. Structures of PEDOT:PSS (left) and PTT:Nafion (right) Illustrating the Polaron for Each Polymer

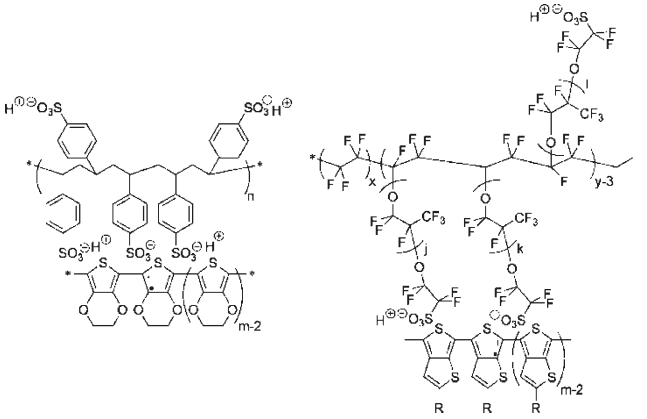

depend sensitively on aspects of its microstructure, such as the degree of order or the presence of substrate-relative orientation and complicate the analysis.

The sensitivity of optical properties to microstructure in polymers has caused SE to be extensively applied to the study of the structure of neat, conjugated polymer films, in the context of both organic LEDs and organic thin-film transistors. It is well established that for many systems, in particular the polythiophenes,[15] poly(arylenephenylenes),[16] and polyfluorenes,[17] the optical properties of the film are highly anisotropic due to a preference for the chain long axis to orient parallel to the plane of the substrate. The characterization of any uniaxial material (having one distinct optical axis, the *c*-axis) with *c*-axis parallel to the surface normal is problematic, particularly for high refractive index systems, because ellipsometry is primarily sensitive to the "projection of the dielectric tensor onto the line of intersection between surface and plane of incidence".[18] For thin films, the presence of reflected waves increases the contrast in *c*-axis uniaxial films, but correlations will often preclude robust analysis of measurements on a single substrate.

This issue is typically addressed with a multisample analysis that combines data from either multiple film thicknesses[19] or identical films on different substrates.[20] We have employed the multiple substrate approach, acquiring data from three nominally identical (contemporaneously deposited) films on three substrates: a Si wafer with a thin native oxide surface layer, a Si wafer with a ≈ 200 nm thick thermally grown oxide surface layer, and a fused quartz slide. In an optimized BHJ device the active layer is typically optically thick to maximize the absorption of photons. The optical thickness of these films can dramatically reduce the reflected beam intensity over the visible parts of the spectrum used in SE, making interrogation of the buried interface challenging. We have therefore chosen to study the vertical composition profile in films of ≈80 nm thickness prepared in an identical manner to the ≈220 nm thick films we used for devices. The thinner films produce devices with reasonably high efficiency (≈70% of the optimal),[21] yet are thin enough permit measurement of the buried interface. Despite the lower optical thicknesses of our films, we find that the statistical significance of the buried interface characteristics to be marginal. Therefore, we have additionally acquired SE data through the fused quartz from the "reverse" side, which significantly improves the precision of the extracted buried interface parameters.

Early SE studies of BHJ layers[22] established that device-relevant blend films are optically anisotropic. However, in most studies of the optics of these devices, isotropic dielectric

Scheme 3. Models Used for the Three Substrates (From Top to Bottom: Native Oxide, Thermal Oxide, and Fused Quartz

EMA P3HT and PCBM (%P3HT$_t$, t$_{top}$)
EMA P3HT and PCBM (%P3HT$_m$, t$_1$)
EMA P3HT and PCBM (%P3HT$_b$, t$_{bot}$)
HTL if present (t)
Native SiO_2
Si

EMA P3HT and PCBM (%P3HT$_t$, t$_{top}$)
EMA P3HT and PCBM (%P3HT$_m$, t$_1$)
EMA P3HT and PCBM (%P3HT$_b$, t$_{bot}$)
HTL if present (t)
Thermal SiO_2 (t = 200 nm)
Si

EMA P3HT and PCBM (%P3HT$_t$, t$_{top}$)
EMA P3HT and PCBM (%P3HT$_m$, t$_1$)
EMA P3HT and PCBM (%P3HT$_b$, t$_{bot}$)
HTL if present (t)
Fused Quartz

function models are assumed. Vertical segregation has recently been included in optical models of blend layers,[12] but it was included with an isotropic dielectric function. In this work, we account for both the optical anisotropy and vertical segregation to develop an accurate physical model for the blend layer. Shown in Scheme 3 are the models adopted for each of the three substrates employed. We have subdivided the BHJ blend layer into three sublayers, including two interfacial sublayers and a center or bulk sublayer, to account for vertical segregation. This approach is more flexible than the linear gradient assumed in earlier work.[12] We find this added flexibility to be essential to the description of films on low γ substrates. In the multiple sample analysis, the optical function for the three BHJ sublayers are assumed identical for the three samples. Similarly, the thicknesses of the top and bottom interface sublayers are assumed to be the same for all three samples, with minor film to film variability being accounted for by allowing independent fitting of the middle sublayer thickness. The middle sublayer thickness varied by less than 13% across the three samples.

The dielectric functions of the Si, native oxide, thermal oxide, and fused quartz were taken from the literature.[23] The dielectric functions for the HTLs were measured from neat HTL films cast on the three substrates. Shown in Figure 1 are the complex refractive indices $N = n + ik$ for the two HTLs, resolved in the directions parallel (x, y) and perpendicular (z) to the plane of the film. The PEDOT:PSS index of refraction is similar to previous reports.[24] Notably it exhibits moderate anisotropy, particularly in the near-infrared (NIR) region, that arises from the mobile carriers. The PTT:Nafion index of refraction is slightly lower than that of PEDOT:PSS over most of the spectrum, and noticeably more transparent in the UV region, consistent with the use of Nafion vs PSS as the dopant. PTT:Nafion also exhibits anisotropy in its NIR index of refraction. The thicknesses of the oxide and HTL layers in the multisample analyses were determined by fits to reference films and held fixed during subsequent analyses.

The dielectric functions of the three BHJ sublayers were modeled with a linear effective medium approximation (EMA) mixture of PCBM and P3HT. The PCBM dielectric function was assumed to be isotropic, whereas P3HT was allowed to be anisotropic: uniaxial with the c-axis parallel to

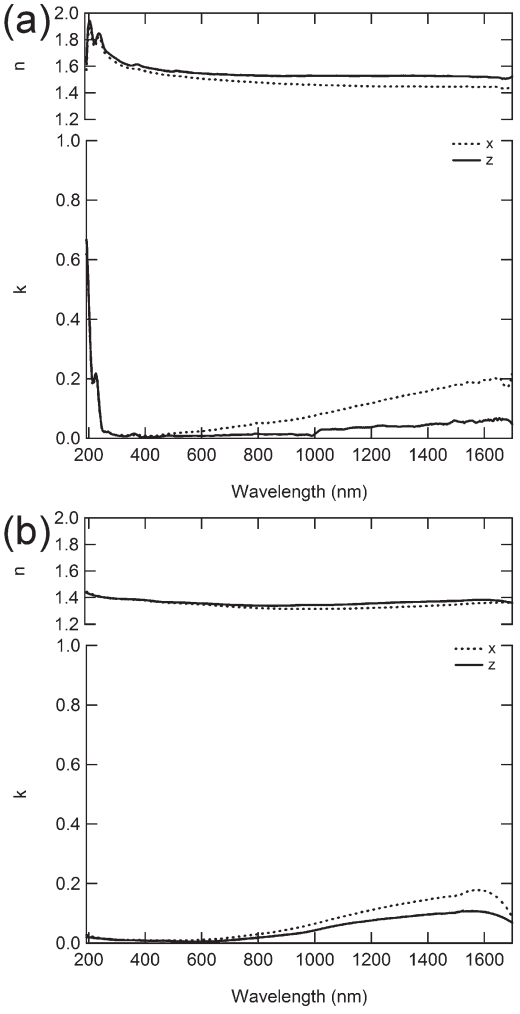

Figure 1. Derived index of refraction ($n + ik$) for (a) PEDOT:PSS and (b) PTT:Nafion illustrating the weak anisotropy of both films in the NIR and the greater transmission of the PTT:Nafion film in the UV.

the substrate normal, consistent with expectations based on spun-cast neat P3HT films.[22] The dielectric function for PCBM was derived from pure PCBM reference films where the dielectric function was solved without any *a priori* assumptions and was found to be similar to that reported in the literature (see Supporting Information).[25,26] In contrast to PCBM, P3HT has an absorption spectrum that strongly depends on processing. A fundamental understanding of the relationship between local order and the vibronic structure in P3HT absorption is emerging,[27] but it remains impractical to develop a robust optical model from first principles. We have therefore chosen to develop an entirely empirical, yet flexible, optical model for P3HT that is based on the well-known sensitivity of the P3HT film structure to processing conditions.[28] Our P3HT optical model was developed by combining the dielectric functions of a library of three reference films that were prepared by varying casting conditions. The three films represent extremely ordered P3HT (well-resolved vibronic features and strong anisotropy), extremely disordered P3HT (weak vibronic features and little anisotropy), and an intermediate case (Figure 2a). The uniaxial P3HT refractive index ($N_x = N_y \neq N_z$) was then taken as a linear EMA mixture of these three P3HT basis films with the volume fraction fit to the BHJ under analysis. Attempts to use highly flexible, causal dielectric functions to represent the polymer generally failed

due to strong correlations between the parameters. While the EMA will not represent nonadditive features in the dielectric function, such as below gap, charge transfer absorption bands,[29] these features are in general weak and should not significantly affect the dielectric function at the precision of the measurement.

Extreme care must be exercised when interpreting SE models to avoid either overfitting the data or reaching a false conclusion based on a best fit to a physically incorrect model. We have attempted to address these issues by analyzing the relative improvements in the key features of our optical model: blend anisotropy and vertical composition. We also validated the SE model fit conclusions using model-independent probes of the order/crystal orientation (GIXD) and interface composition (NEXAFS) when possible.

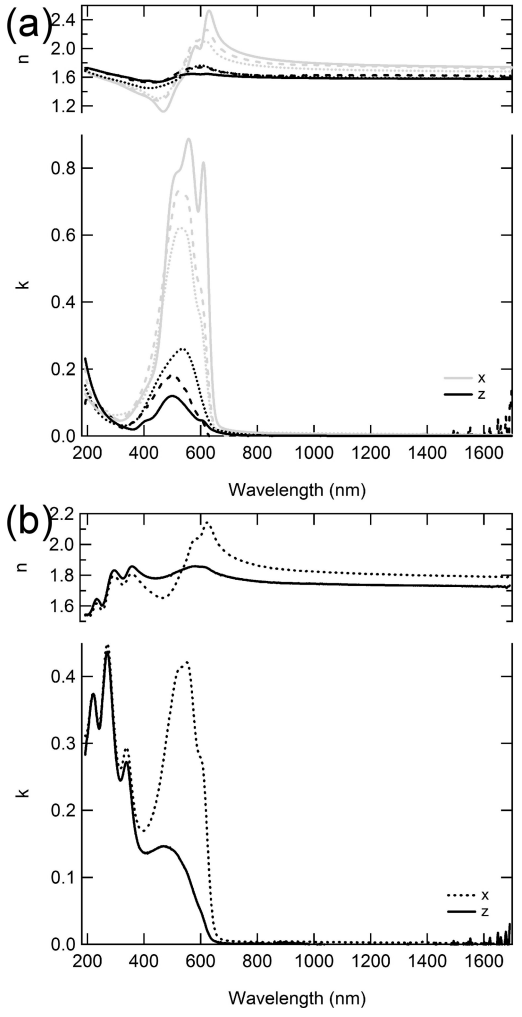

Figure 2. In-plane (x) and out-of-plane (z) index of refraction ($n + ik$) for (a) the three, experimentally derived, P3HT functions that were the basis for the EMA model and (b) the best-fit refractive index for an exemplar blend film on SiO_2 showing a high degree of anisotropy.

As with the XPS measurements described earlier,[14] NEXAFS analysis could not be performed on the PEDOT:PSS buried interface due to cohesive failure in the HTL. Therefore, blend films were also cast onto high-γ SiO_2 substrates that are amenable to active layer delamination to serve as an additional test of the ellipsometric model that could be validated using NEXAFS.

The results of the optimized three sublayer model fit to the P3HT:PCBM blend film on SiO_2 are shown in Table 1 and Figure 3. The results indicate a PCBM-rich buried interfacial sublayer, an intermediate bulklike region with ≈60 vol % P3HT, and a P3HT-rich sublayer at the air interface. The fullerene enrichment at the buried interface is consistent with expectations based on earlier studies of high γ substrates; the polymer enrichment at the air interface is also consistent with expectations.[8,14] Accurate densities for either P3HT or PCBM are not known at this time; however, assuming typical values (ρ_{P3HT} = 1.1 g/mL and ρ_{PCBM} = 1.3 g/mL), the original solution mass ratio is consistent with the observed bulk volume fraction. Shown in Figure 2b is the best fit dielectric function for the middle sublayer of the film, indicating the clear anisotropy of the polymer (absorption near ≈500 nm), consistent with a preference for in-plane orientation of the long chain axis. Also clear in the dielectric function is the distinct vibronic structure in the P3HT, characteristic of semicrystalline material and typically diagnostic of high performing BHJs.[30] The correlation between P3HT order and solar cell efficiency has been generally attributed to improved hole mobility in the polymer upon ordering. The derived dielectric function from our optimized

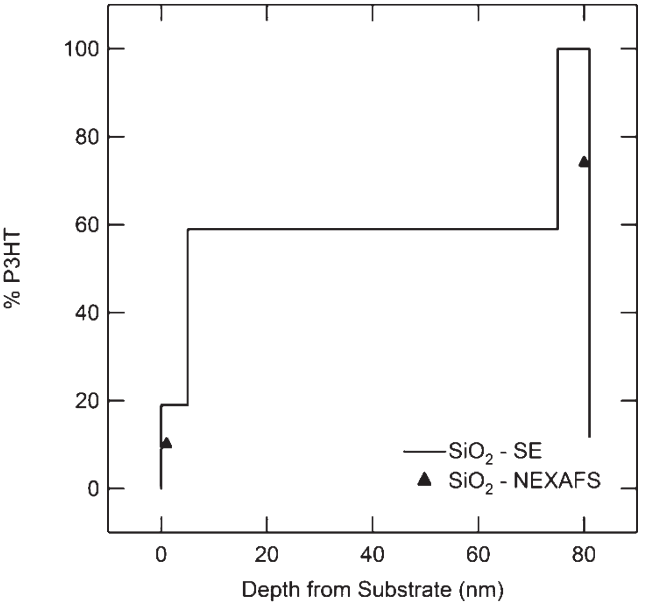

Figure 3. Plot of P3HT volume fraction as a function of depth for P3HT:PCBM blend film on SiO_2 substrates as determined by the optimized VASE model (line) with composition data from NEXAFS spectroscopy (markers).

Table 1. Comparison of Interface Composition by NEXAFS and VASE and Layer Thicknesses by VASE

	top			middle		bottom		
	% $P3HT_N$[a]	% $P3HT_{SE}$[b]	t_{SE} [nm]	% $P3HT_{SE}$	t_{SE} [nm]	% $P3HT_N$	% $P3HT_{SE}$	t_{SE} [nm]
SiO_2	74 ± 2	100 ± 1	6 ± 1	59 ± 1	70 ± 4	10 ± 0.2	19 ± 2	5 ± 1
PEDOT:PSS	74 ± 2	100 ± 1	6 ± 1	59 ± 1	70 ± 1	n/a	46 ± 1	16 ± 1
PTT:Nafion	75 ± 2	100 ± 1	6 ± 1	57 ± 1	80 ± 1	80 ± 2	88 ± 2	3 ± 1

[a] Error in the NEXAFS data represents the instrumental error of 2%. [b] Error in the SE data represents the 90% confidence limit for each model as determined by Monte Carlo analysis.

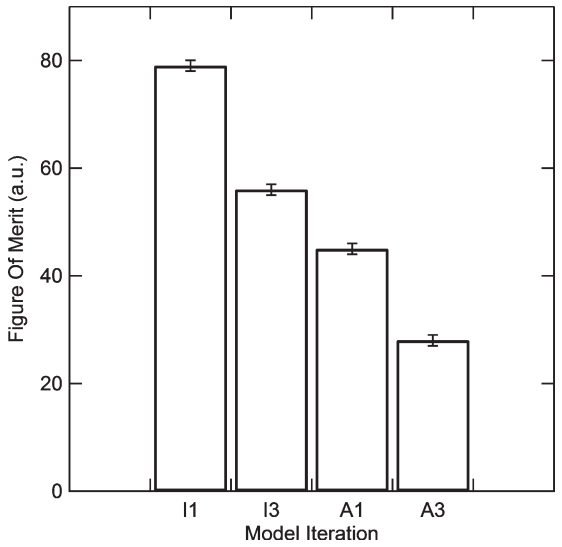

Figure 4. Figure of merit for each iteration of the model for the P3HT:PCBM blend on SiO_2 substrate, where I1, I3, A1, and A3 correspond to isotropic 1-layer, isotropic 3-layer, anisotropic 1-layer, and anisotropic 3-layer models, respectively. The error bars represent the 90% confidence limit for each model as determined by Monte Carlo analysis.

model is consistent with one from a model that does not impose an EMA (like that of Zhokhavets et al.[22]), indicating that the EMA adequately represents the blend.

We confirmed that the complexity of our SE model is justified by comparing how well simpler models could fit the data for films cast onto SiO_2 substrates. The figure-of-merit (FOM) for model fit is the weighted root-mean-squared error (eq 2) where X is the total number of ellipsometric parameter (Ψ, Δ) pairs for all samples and angles, M is the number of fit parameters, and σ is the standard deviation for each data point. As shown in Figure 4, the FOM is reduced by the evolution of the model toward increasing complexity: an isotropic one-layer (I1), an isotropic three-layer (I3), an anisotropic one-layer (A1), and finally an anisotropic three-layer (A3). Clearly, the A3 (anisotropic three-layer) model provides the best fit to the data for our P3HT:PCBM blend films. The greatest improvement in quality of fit is achieved by the inclusion of anisotropy rather than segregation, as the single-layer anisotropic model (A1) has a lower FOM than the three-layer isotropic model (I3). This result implies that the dominant deviation from a simple optical response is the anisotropy and that the vertical segregation, while significant, represents a smaller perturbation.

$$\mathrm{FOM} = \sqrt{\frac{1}{2X - M}\sum_{i-1}^{X}\left[\left(\frac{\psi_i^{\mathrm{mod}} - \psi_i^{\mathrm{exp}}}{\sigma_{\psi,i}^{\mathrm{exp}}}\right)^2 + \left(\frac{\Delta_i^{\mathrm{mod}} - \Delta_i^{\mathrm{exp}}}{\sigma_{\Delta,i}^{\mathrm{exp}}}\right)^2\right]} \quad (2)$$

In order to gain further insight into the ability of the optimized model to detect and model the weak perturbation due to vertical segregation, parametric cuts (often termed uniqueness scans) through the multiparameter FOM space were performed. Shown in Figure 5 are the uniqueness scans for the top and bottom interface sublayer thicknesses. In each scan, the appropriate thickness was varied parametrically with fixed composition while all other model parameters were allowed to adjust to minimize the FOM. In all optimized fits, the best case FOM differs significantly from the ideal of 1, indicating the presence of model deficiencies,

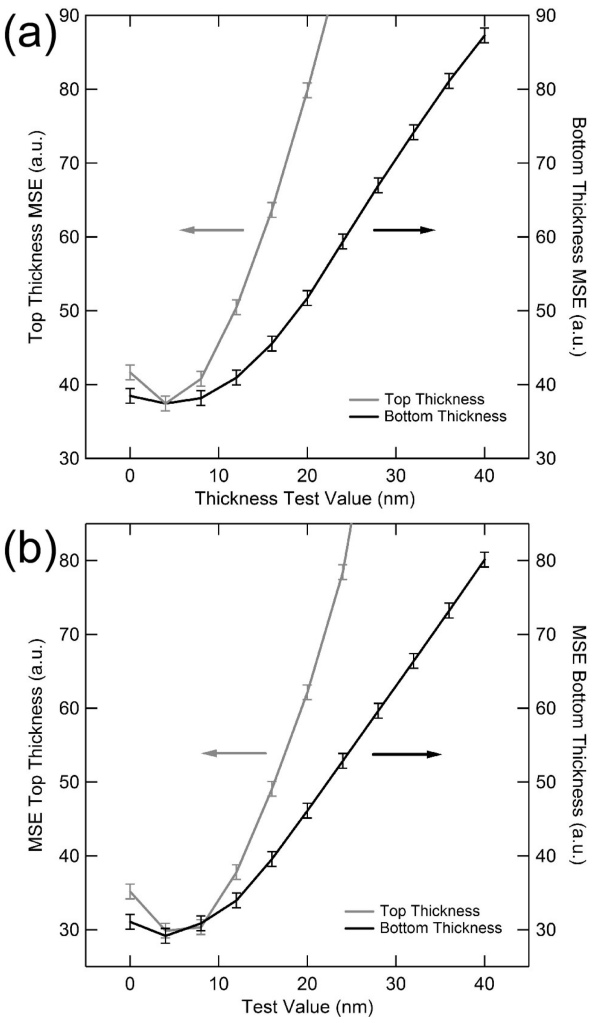

Figure 5. Uniqueness scans of the air and buried interface layer thicknesses for (a) P3HT:PCBM blend film on PTT:Nafion and (b) P3HT:PCBM blend film on SiO_2. Error bars represent the confidence limits of the uniqueness scans as defined by the 90% confidence limit for the bottom layer thickness for each optimized model as determined by Monte Carlo analysis.

systematic instrument errors, or an inaccurate description of the data statistics. This nonideality is typical for most SE measurements and makes application of standard statistical metrics to the question of confidence limits problematic. The "sharpness" of the minimum in FOM was qualitatively assessed by performing Monte Carlo (MC) studies of the model fits by resampling (with replacement) the data on a per spectrum basis. Also shown in Figure 5 is the variance in the FOM from a MC sample of 100 generated SE data sets. Comparison of the FOM variance to the sensitivity with layer thickness indicates that both the top and buried interface sublayers represent statistically robust improvements in the model.

Results from the SE analyses of the P3HT:PCBM blend on the two HTLs are also given in Table1. The volume fraction profiles are given in Figure 6. The overall observations are consistent with expectations based on simple free energy arguments. For both HTLs, as on the oxide substrate, the air interface was polymer-rich. On the low-γ PTT:Nafion, the buried interface is also polymer-rich, consistent with earlier observations on low-γ self-assembled monolayer (SAM)-treated substrates.[8,12] On PEDOT:PSS that has an intermediate γ of $\approx$45 mN/m^2,[31] a composition of $\approx$46% P3HT

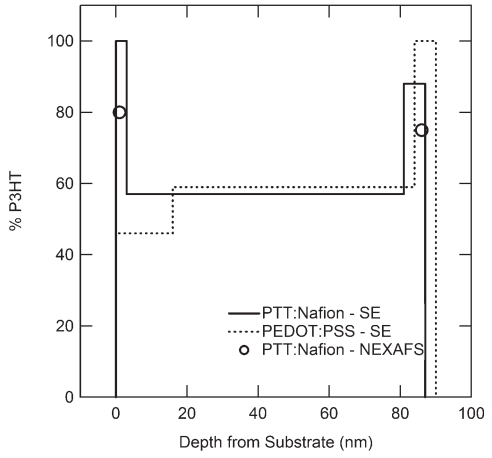

Figure 6. Plot of PCBM composition as a function of depth for P3HT:PCBM blend films on PEDOT:PSS and PTT:Nafion substrates as determined by the optimized VASE model with composition data from NEXAFS spectroscopy for the PTT:Nafion overlaid.

was obtained, intermediate between that of SiO_2 (≈72 mN/m^2) and PTT:Nafion (≈23 mN/m^2).

The results of our modeling for the P3HT:PCBM blend on SiO_2 are consistent with those reported earlier using an isotropic optical model and a constrained linear film profile.[12] However, the level of segregation at each interface predicted by the three-layer model is greater than that obtained with the linear assumption, consistent with the relatively thin sublayer thicknesses derived from SE. The linear model will conform to an "average" composition and thus underestimate the level of segregation. The results of our modeling for the low-γ PTT:Nafion buried interface are also consistent with the earlier optical modeling of SAM-treated substrates. However, the air interface composition in the earlier study was reported to be significantly PCBM-rich, contrary to what was observed here. This discrepancy can be attributed to the inability of a linear model to fit the U-shaped composition profile of the low-γ systems. We have extensively studied the air interface with NEXAFS over a variety of film thicknesses and processing conditions and always find the air interface polymer-rich. We note that numerical studies of vertically homogeneous, but anisotropic, BHJ films result in significant vertical gradients when fit to an isotropic, graded model (see Supporting Information).

A limitation of the optical model employed is that the same P3HT optical function is used throughout the film. Thus, while the model can capture vertical composition gradients, it cannot reflect vertical changes in the polymer order. Recent transmission electron microscopy (TEM) tomography studies have suggested that the density of highly crystalline P3HT wires varies with depth.[32] The interface layers for the films in this report are too thin to enable independent modeling of the polymer dielectric function. However, in preliminary studies of films cast from chlorobenzene, which produces significantly less ordered films, we do find it necessary to allow the P3HT in the bulk of the film to adopt an anisotropy and order distinct from those of the surface region. This significantly complicates the modeling. It is clear that the specifics of the polymer order and any vertical gradient therein will significantly depend on film processing.

Grazing Incidence X-ray Diffraction. Our modeling of the SE data reveals that the BHJ films are highly anisotropic with thin interface regions having compositions that deviate significantly from the bulk. To confirm these principal

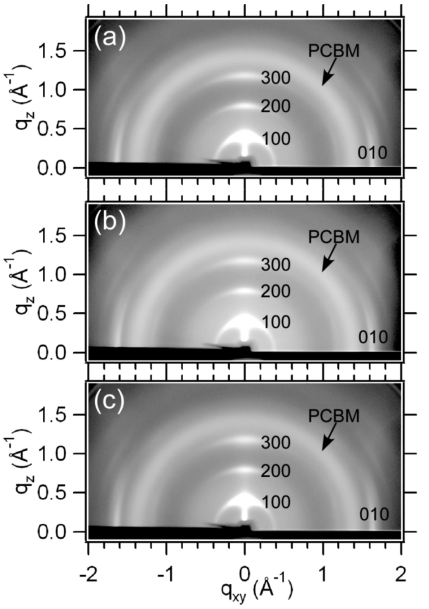

Figure 7. GIXD images of P3HT:PCBM blend films on (a) SiO_2, (b) PEDOT:PSS, and (c) PTT:Nafion showing oriented P3HT domains.

structural observations, grazing-incidence X-ray diffraction (GIXD) and near-edge X-ray absorption fine structure (NEXAFS) spectroscopy measurements were performed. Shown in Figure 7 are GIXD images recorded on each of the three substrates: SiO_2, PEDOT:PSS, and PTT:Nafion. No significant difference in the degree of crystalline order or crystal orientation was observed among the three substrates. In each case, the (100), (200), and (300) P3HT lamellar peaks were preferentially oriented normal to the sample, and the (010) P3HT π-stacking peak was oriented in-plane. This crystal orientation arises from an edge-on orientation of the P3HT conjugated planes with the P3HT long axes in-plane, consistent with both the high degree of fine structure and the anisotropy observed in the SE. The d-spacing ($d_{100} \approx$ 1.55 nm and $d_{010} \approx 0.38$ nm) are identical to those measured for a neat film of the same molecular weight P3HT, indicating no significant perturbation of the P3HT ordered domains by the addition of fullerenes. The radial arcs extending from the P3HT diffraction peaks indicate a significant distribution of crystal orientations centered about the a-axis orientation. The diffuse ring at ≈1.4 Å^{-1} is due to scattering from the PCBM. The uniform intensity of the ring indicates no preferential order of the PCBM domains, consistent with our earlier assumption of an isotropic dielectric function for the fullerene.

NEXAFS Spectroscopy. Partial electron yield (PEY) NEXAFS spectra are shown in Figure 8 recorded for the air interface of P3HT:PCBM blend films spun-cast upon the three substrates: SiO_2, PEDOT:PSS, and PTT:Nafion. Also shown are reference spectra for the pure components P3HT and PCBM. It is clear that no significant variation in the composition with change in substrate γ was detected; the air interface was polymer-rich in all cases. The interface compositions can be quantified assuming that the mean free path of both photons and electrons through PCBM and P3HT are equivalent; a blend spectrum can then be fit to a linear combination of pure component spectra weighted by volume fraction. Independent of substrate treatment, the least-squares fitting indicates the air interfaces were 75%−80% P3HT. The results are summarized in Table 1 and Figures 4 and 6. The reported uncertainties are one standard deviation

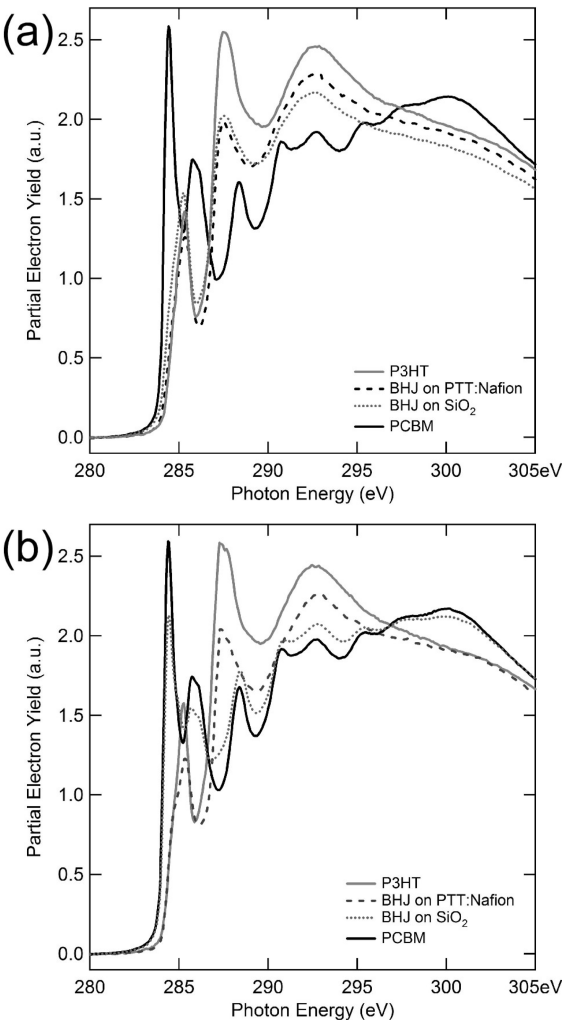

Figure 8. NEXAFS spectra of the (a) air interface and (b) the buried interface for the BHJ films on SiO_2 and PTT:Nafion bracketed by the P3HT and PCBM control film spectra illustrating the P3HT-enriched air interface in all cases and the change in composition at the buried interface with change in γ.

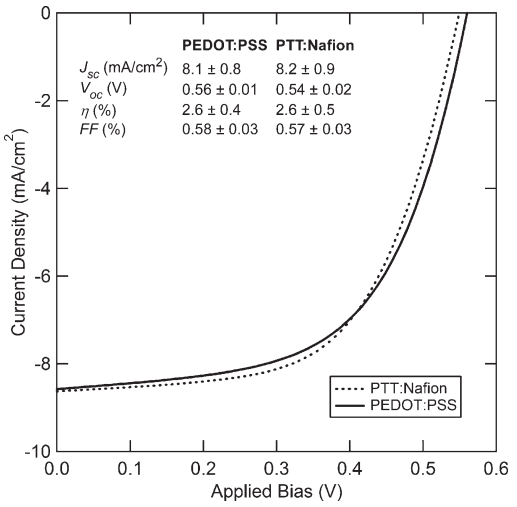

Figure 9. $J-V$ curves for the P3HT:PCBM BHJ devices prepared on PTT:Nafion and PEDOT:PSS (curves corrected for the spectral mismatch factor) and the average device performance for eight devices (J_{sc}, V_{oc}, η, and FF) in table (inset). Error in the device performance data represents the standard deviation over eight devices.

over three independent sample series. The PEY spectra were collected with a grid bias of −50 V, providing a surface-weighted signal such that ≈50% originates within 2 nm of the interface and ≈75% originates within 4 nm.[33] The estimated air interface sublayer thickness from SE is therefore large compared to the sampling depth of the NEXAFS, so direct comparison of SE and NEXAFS is possible. The NEXAFS and SE data are in good qualitative agreement on the enrichment of the polymer at the air interface. The SE appears to overestimate the polymer fraction perhaps due to the influence of surface roughness. Because the polymer was the lower index material, excess polymer will approximate a significant void fraction (surface roughness). Explicit inclusion of surface roughness, in the form of a 50% EMA model of blend and void, did not improve the SE model.

The buried interfaces were measured by NEXAFS spectroscopy after exposure via delamination as described previously.[8] The former substrates were also evaluated to check the quality of the delamination. For both the SiO_2 and PTT:Nafion substrates, no P3HT or PCBM residue could be observed, suggesting clean adhesive failure at the buried interface. The clean delamination from PTT:Nafion was consistent with our earlier experience with low-γ substrates. Unfortunately, as reported earlier,[8,14] clean delamination of the PEDOT:PSS interface could not be achieved. Attempts to rinse excess PEDOT:PSS off the delaminated P3HT:PCBM film by various methods proved unsuccessful. Shown in Figure 8 are the buried interface NEXAFS spectra for the SiO_2 and PTT:Nafion. The buried interface spectra show clear changes in composition as a function of substrate γ; P3HT volume fractions of 10% and 80% are obtained for the SiO_2 and PTT:Nafion, respectively. These values are also summarized in Table 1. There was good quantitative agreement between the NEXAFS and SE buried interface compositions, confirming the applicability of the developed SE model and providing confidence in the SE derived values for the PEDOT:PSS interface which can only be addressed nondestructively.

The orientation of the polymer 1s → π^* director was also assessed for both the air and buried interfaces of those sublayers that were polymer-rich (see Supporting Information) by determination of the dichroic ratio R ($R = -1$ for π^* normal to the surface and $R \approx 0.7$ for edge-on). In all cases, R was ≈0.2, indicating a preferentially edge-on conjugated plane. These results provided additional confirmation of orientation in the P3HT:PCBM blend films, consistent with the orientation of P3HT crystals in GIXD and the high level of long axis order implied by the optical anisotropy.

OPV Devices. As illustrated in Figure 9, there was no appreciable difference in performance between devices prepared on PTT:Nafion and PEDOT:PSS. All devices tested in this study performed within the expected norms for devices of this architecture and cathode composition (LiF/Al).[34] Notably, the expected improvement in short-circuit current (J_{sc}) for the device spun on PTT:Nafion, which had a P3HT-enriched buried interface was not observed.

While the SE investigation clearly establishes a significant difference in the buried interface composition for devices upon PEDOT:PSS vs PTT:Nafion, the difference was not relevant in these devices. The derived P3HT buried interface volume fraction of 47% appears to be adequate for high initial performance. In retrospect, this was not surprising as the observed volume fraction was nearly that of the bulk device, and presumably the slight excess amount of PCBM does not represent a significant barrier to hole transport. It is interesting to note that the P3HT domains in this sublayer, as

with the whole of the film, are oriented in a transistor-like orientation (edge-on relative to the substrate normal) which allows for efficient transport of charges *parallel* to the planar anode so that charges could find alternative conduction pathways when blocked by a PCBM domain. We also note that the water contact angle of PEDOT:PSS is time-dependent, indicating reasonably facile reorganization of the surface and thus a dynamic, processing-dependent interface structure. This is in contrast to PTT:Nafion which exhibits a very stable water contact angle. Thus, the absence of device significant interface segregation at the PEDOT:PSS interface may be due, in part, to an "amphiphilic" dynamic interface.

These results provide additional context for the observations reported by Xu et al. that inverted devices (where the cathode is at the buried interface and the anode at the air interface of the active layer) perform better than conventional devices due to γ directed segregation of the blend components into optimal interfacial layer compositions (PCBM enrichment at the cathode and P3HT enrichment at the anode). It appears clear that the improvement reported for the inverted device, if due to interface effects, is likely due to the improvement of the air (anode/inverted, cathode/normal) interface composition. This conclusion is additionally supported by the recent work of Wei and Kumar, where buffer layers of PCBM were engineered at the air interface of the blend film (by preferential segregation or evaporation of fullerenes, respectively).[35,36] These results suggest that, from an initial performance optimization perspective, there is greater gain from engineering the cathode interface for conventional devices than engineering the anode interface. We note that the conventional devices reported here have nominally identical performance to the inverted devices reported by Xu et al. Similarly, the best performance for optimized conventional P3HT:PCBM- and PEDOT:PSS-based devices is nominally identical to that of optimized inverted devices.[14,34,37] Thus, it maybe that the ≈25% PCBM composition consistently reported for the air interface of this blend is adequate for good initial performance and the improved device performance upon interface engineering may originate from band offset, interface dipole effects, or additional factors other than the interfacial segregation that clearly occurs.[38,39]

Conclusions

We have presented a detailed optical model for P3HT:PCBM BHJ films that accounts for both optical anisotropy and vertical segregation. It is capable of describing segregation at both the air and buried interfaces. We demonstrate that the buried interface composition on PEDOT:PSS layers are only slightly enriched with PCBM and that a low γ Nafion-based HTL can cause the buried interface to become P3HT-rich. Even though the buried interface composition did not influence the performance of our devices, it is clear that understanding the interfacial segregation of BHJ active layer blends is important for device optimization. However, it is also clear that interface effects may be subtle, and accurate measurements of composition and orientation in BHJ active layer blends must be employed to develop a complete understanding of how device architecture and materials choices affect device performance.

Experimental Section

Materials. P3HT (Plexcore 2100, Plextronics Inc., Pittsburgh, PA)[40] and PCBM (99.5%, Nano-C Inc., Westwood, MA) were used as received. PEDOT:PSS (Clevios P VP Al 4083, H.C. Starck Inc., Newton, MA) and PTT:Nafion (Product No. YCD-321-064, Air Products Inc., Allentown, PA) were filtered through 0.22 μm PVDF syringe filters prior to use and stored in a refrigerator when not in use. Isopropyl alcohol (anhydrous, Warner-Graham Co., Cockeysville, MD), Parylene-C (Specialty Coating Systems, Indianapolis, IN), acetone (HPLC grade), toluene (anhydrous), chloroform (HPLC grade), and 1,2-dichlorobenzene (anhydrous, Sigma-Aldrich, St. Louis, MO) were used as received. Prime grade, single side polished silicon wafers (N-type, phosphorus doped, ⟨100⟩ orientation) (Montco Silicon, Spring City, PA) and prime grade silicon wafers with 200 nm SiO_2 were prepared at the NIST Nanofab, and fused quartz slides were purchased from GM Associates (Oakland, CA). Prepatterned indium−tin oxide (150 ± 7.5 nm thickness, sheet resistance $< 20 \pm 5$ ohms/square, and 88% transmission at 550 nm) on Eagle 2k glass chips (1 in.) were prepared by Thin Film Devices, Inc. (Anaheim, CA).

Methods. All substrates were cleaned by sonication for 10 min in acetone, then isopropyl alcohol, and followed by treatment for 10 min under UV-ozone, immediately followed by a water rinse with ultrapure water and drying under ultrapure, dry N_2. All substrates were used within 30 min of cleaning.

PEDOT:PSS films were prepared by spin-casting at 5000(2π) rad/min for 60 s followed by thermal treatment at 120 °C for 20 min in an inert atmosphere. PTT:Nafion films were prepared by spin-casting at 2500(2π) rad/min for 60 s followed by thermal treatment at 180 °C for 10 min in an inert atmosphere. All HTL films were used within 1 h of fabrication.

P3HT:PCBM blend films were prepared in a manner similar to that reported by Li et al. under inert atmosphere conditions.[37] For structural characterization 15 g/L (total solids) solutions in 1,2-dichlorobenzene (with a P3HT:PCBM mass ratio of 1:1) were heated overnight at 80 °C. Blend films were spun at 500(2π) rad/min for 60 s with an acceleration of 84(2π) rad/(min s). The resultant still-wet films were allowed to dry over ≈20 min on a level stage under a Petri dish lid. Films for device studies were spun in the same manner from 30 g/L (total solids) solutions. OPV devices were fabricated on PEDOT:PSS or PTT:Nafion treated patterned ITO in the same manner as the nonfunctional P3HT:PCBM blend films. The metallic top contacts (typically 1.5 nm LiF and 100 nm Al) were deposited using a thermal evaporator (MBraun), chamber-locked in an inert atmosphere glovebox, and completed devices were then sealed in aluminized Mylar bags and transferred to a separate inert atmosphere box for performance testing in the manner reported by Shrotriya et al.[41] $J-V$ curves were measured under an Ar atmosphere using an Agilent 4155C parameter analyzer. The photocurrent was measured under AM1.5G 100 mW/cm^2 illumination from a Thermo Oriel 96 000 150 W solar simulator that was filtered through a neutral density filter and an AM1.5G filter (Model AM0, Oriel Corp., Stratford, CT) and then transferred into the box via a liquid light guide (Model 77637, Newport Corp., Irvine, CA). The light intensity was determined using a thermopile and power meter combination (PowerMax PS19 thermopile and Fieldmate Laser power meter, Coherent Inc., Santa Clara, CA), and the OPV device performance was referenced to a monosilicon photodiode fitted with a KG-5 visible color filter (Model S1133, Hamamatsu) calibrated by the National Renewable Energy Laboratory (NREL). All efficiency values reported in this work were corrected by the spectral mismatch factor.

Films for delamination were placed in a PDS-2010 (Specialty Coating Systems, Indianapolis, IN), and 10 g of Parylene-C was evaporated resulting in a film thickness of ≈10 μm. The parylene films were then trimmed off of the edges of the samples with a scalpel and were delaminated directly (low γ) substrates, or the interface was broken by immersion in water for 12 h. The former substrates were retained for NEXAFS spectroscopy analysis.

Surface energy determination of PTT:Nafion was performed with an FTA125 contact angle system (First Ten Angstroms, Inc., Portsmouth, VA). Three liquids were employed (water, ethylene glycol, and formamide), and contact angles for each liquid were taken as the average value of four independent

drops. The surface energy was determined using the provided software (FTA32) and was taken as the average calculated for all three liquids using the extended Girifalco−Good−Fowkes−Young method which is an adaption of the Girifalco−Good−Fowkes−Young method for low-γ surfaces by calibration with water on poly(tetrafluoroethylene).

NEXAFS spectroscopy was performed at the National Institute of Standards and Technology soft X-ray materials characterization facility (beamline U7A) at the National Synchrotron Light Source (NSLS) of Brookhaven National Laboratory. Orientation was characterized by collecting carbon K-edge spectra in partial electron yield (PEY) mode with a grid bias of −50 V. The experimental standard uncertainty in the peak position for PEY spectra was 0.15 eV; the yield uncertainty was ≈2%. Incident angles Θ (with respect to the surface plane) were varied at five angles: 20°, 33°, 44°, 54.7°, and 70°. The $1s \rightarrow \pi^*$ intensity was fit to a linear dependence on $\sin^2 \Theta$. This fit was used to extrapolate intensities at 0 and 90° incidence, which were then used to calculate the figure-of-merit $R = (I(90°) - I(0°))/(I(90°) + I(0°))$.

Grazing incidence X-ray diffraction (GIXD) was performed at beamline 11-3 at the Stanford Synchrotron Radiation Laboratory using a two-dimensional image plate detector. Data were collected at incident angles of ≈0.1° at an energy of 12.72 keV. The sample-to-detector distance was determined with a LaB_6 calibration sample.

Ellipsometric data were collected at multiple angles depending on the substrate the film was cast upon (45°, 60°, and 75° for Si with native and 200 nm SiO_2 and 45°, 52.5°, 60°, 67.5°, and 75° for fused quartz). Four measurements were made on identical films on three substrates: Si wafers terminated with native SiO_2, 200 nm thick thermally grown SiO_2, and fused quartz with the beam incident from the film side and the substrate side of the sample. For measurements on fused quartz with the beam incident on the film side of the sample the back reflection of the clean side of the substrate was minimized by index matching to a piece of opaque tape (Magic Tape, 3M Corp., Minneapolis, MN). Additionally, the light incident on the surface was weakly focused to a ≈300 μm diameter spot, using vendor supplied focusing optics to reduce the effect of film heterogeneity and, for the measurements with fused quartz substrates, to aid in the isolation of the light reflected from the desired surface (film-side or substrate-side). All data were obtained with an M-2000D series spectroscopic ellipsometer (J.A. Woollam Inc., Lincoln, NE). All data sets were then fit simultaneously using vendor supplied analysis software (WVASE32).

Acknowledgment. Research performed in part at the NIST Center for Nanoscale Science and Technology. The authors thank Air Products Inc. for the donation of PTT:Nafion. The authors also thank Drs. Christopher L. Soles and Eric K. Lin for scientific discussions during the preparation of this manuscript. D.S.G. and C.K.C. thank the National Research Council Research Associateship Program at NIST for financial support. Portions of this research were carried out at the Stanford Synchrotron Radiation Lightsource, a national user facility operated by Stanford University on behalf of the U.S. Department of Energy, Office of Basic Energy Sciences.

Supporting Information Available: Figures depicting the complex index of refraction for PCBM, and P3HT:PCBM blend, representative plots of ellipsometric parameter Ψ and fits to the data for a graded, isotropic model vs the optimized anisotropic, three-layer model, and plots of the dichroic ratio for the P3HT:PCBM blend film orientation. This material is available free of charge via the Internet at http://pubs.acs.org.

Note Added after ASAP Publication. This article posted ASAP on March 25, 2010. Figures 1, 2, 6, and 9 have been revised. The correct version posted on March 30, 2010.

References and Notes

(1) Krebs, F. C. *Sol. Energy Mater. Sol. Cells* **2009**, *93*, 394–412.
(2) Gaudiana, R. A.; Brabec, C. *Nat. Photonics* **2008**, *2*, 287–289.
(3) Fan, X.; Chu, Z.; Wang, F.; Zhang, C.; Chen, L.; Tang, Y.; Zou, D. *Adv. Mater.* **2008**, *20*, 592–595.
(4) O'Connor, B.; Pipe, K. P.; Shtein, M. *Appl. Phys. Lett.* **2008**, *92*, 193306.
(5) Benanti, T. L.; Venkataraman, D. *Photosynth. Res.* **2006**, *87*, 73–81.
(6) Peet, J.; Senatore, M. L.; Heeger, A. J.; Bazan, G. C. *Adv. Mater.* **2009**, *21*, 1521–1527.
(7) Thompson, B. C.; Fréchet, J. M. J. *Angew. Chem., Int. Ed.* **2009**, *47*, 58–77.
(8) Germack, D. S.; Chan, C. K.; Hamadani, B. H.; Richter, L. J.; Fischer, D. A.; Gundlach, D. J.; DeLongchamp, D. M. *Appl. Phys. Lett.* **2009**, *94*, 233303.
(9) Chen, X.; Gardella, J. A. J. *Macromolecules* **1994**, *27*, 3363–3369.
(10) Iyengar, D. R.; Perutz, S. M.; Dai, C. A.; Ober, C. K.; Kramer, E. J. *Macromolecules* **1996**, *29*, 1229–1234.
(11) Bjorstrom, C. M.; Nilsson, S.; Bernasik, A.; Budkowski, A.; Andersson, M.; Magnusson, K. O.; Moons, E. *Appl. Surf. Sci.* **2007**, *253*, 3906–3912.
(12) Campoy-Quiles, M.; Ferenczi, T.; Agostinelli, T.; Etchegoin, P. G.; Anthopolous, T. D.; Stavrinou, P. N.; Bradley, D. D. C.; Nelson, J. *Nat. Mater.* **2008**, *7*, 158–164.
(13) Liao, H. H.; Chen, L. M.; Xu, Z.; Li, G.; Yang, Y. *Appl. Phys. Lett.* **2008**, *92*, 173303.
(14) Xu, Z.; Chen, L. M.; Yang, G.; Huang, C.-H.; Hou, J.; Wu, Y.; Li, G.; Hsu, C.-S.; Yang, Y. *Adv. Funct. Mater.* **2009**, *19*, 1227–1234.
(15) Gurau, M. C.; Delongchamp, D. M.; Vogel, B. M.; Lin, E. K.; Fischer, D. A.; Sambasivan, S.; Richter, L. J. *Langmuir* **2007**, *23*, 834–842.
(16) Losurdo, M.; Bruno, G.; Irene, E. A. *J. Appl. Phys.* **2003**, *94*, 4923–4929.
(17) Tammer, M.; Higgins, R. W. T.; Monkman, A. P. *J. Appl. Phys.* **2002**, *91*, 4010–4013.
(18) Aspnes, D. E. *J. Opt. Soc. Am.* **1980**, *70*, 1275–1277.
(19) Tammer, M.; Monkman, A. P. *Adv. Mater.* **2002**, *14*, 210–212.
(20) Järrendahl, K.; Arwin, H. *Thin Solid Films* **1998**, *313*, 114–118.
(21) Moulé, A. J.; Bonekamp, J. B.; Meerholz, K. *J. Appl. Phys.* **2006**, *100*, 094503.
(22) Zhokhavets, U.; Erb, T.; Gobsch, G.; Al-Ibrahim, M.; Ambacher, O. *Chem. Phys. Lett.* **2006**, *418*, 347–350.
(23) Herzinger, C. M.; Johs, B.; McGahan, W. A.; Woolam, J. A.; Paulson, W. *J. Appl. Phys.* **1998**, *83*, 3323–3336.
(24) Pettersson, L. A. A.; Ghosh, S.; Inganas, O. *Org. Electron.* **2002**, *3*, 143–148.
(25) Kelly, M. K.; Etchegoin, P. G.; Fuchs, D.; Krätschmer, W.; Fostiropoulos, K. *Phys. Rev. B* **1992**, *46*, 4963–4968.
(26) Richter, W. *Philos. Trans. R. Soc. London, Ser. A* **1993**, *344*, 453–467.
(27) Clark, J.; Silva, C.; Friend, R. H.; Spano, F. C. *Phys. Rev. Lett.* **2007**, *98*, 206406.
(28) DeLongchamp, D. M.; Vogel, B. M.; Jung, Y.; Gurau, M. C.; Richter, C. A.; Kirillov, O. A.; Obrzut, J.; Fischer, D. A.; Sambasivan, S.; Richter, L. J.; Lin, E. K. *Chem. Mater.* **2005**, *17*, 5610–5612.
(29) Vandewal, K.; Goris, L.; Haeldermans, I.; Nesládek, M.; Haenan, K.; Wagner, P.; Manca, J. V. *Thin Solid Films* **2008**, *516*, 7135–7138.
(30) Li, G.; Shrotriya, V.; Huang, J.; Yao, Y.; Moriarty, T.; Emery, K.; Yang, Y. *Nat. Mater.* **2005**, *4*, 864–868.
(31) Wang, X. J.; Ederth, T.; Inganas, O. *Langmuir* **2006**, *22*, 9287–9294.
(32) van Bavel, S.; Sourty, E.; de With, G.; Frolic, K.; Loos, J. *Macromolecules* **2009**, *42*, 7396–7403.
(33) Prabhu, V. M.; Sambasivan, S.; Fischer, D.; Sundberg, L. K.; Allen, R. D. *Appl. Surf. Sci.* **2006**, *253*, 1010–1014.
(34) Reese, M. O.; White, M. S.; Rumbles, G.; Ginley, D. S.; Shaheen, S. E. *Appl. Phys. Lett.* **2008**, *92*, 053307.
(35) Kumar, A.; Li, G.; Hong, Z.; Yang, Y. *Nanotechnology* **2009**, *20*, 165202.
(36) Wei, Q.; Nishizawa, T.; Tajima, K.; Hashimoto, K. *Adv. Mater.* **2008**, *20*, 2211–2216.
(37) Li, G.; Yao, Y.; Yang, H.; Shrotriya, V.; Yang, G.; Yang, Y. *Adv. Funct. Mater.* **2007**, *17*, 1636–1644.
(38) Hau, S. K.; Yip, H.-L.; Acton, O.; Baek, N. S.; Ma, H.; Jen, A. K.-Y. *J. Mater. Chem.* **2008**, *18*, 5113–5119.
(39) Yip, H.-L.; Hau, S. K.; Baek, N. S.; Jen, A. K.-Y. *Appl. Phys. Lett.* **2008**, *92*, 193313.
(40) Certain commercial equipment, instruments, or materials are identified in this paper to foster understanding. Such identification does not imply recommendation or endorsement by the National Institute of Standards and Technology, nor does it imply that the materials or equipment identified are necessarily the best available for this purpose.
(41) Shrotriya, V.; Li, G.; Yao, Y.; Moriarty, T.; Emery, K.; Yang, Y. *Adv. Funct. Mater.* **2006**, *16*, 2016–2023.